

# Modeling OxLDL Epigenetic Innate Immune Training of Monocytes in Early Atherosclerotic Plaques

Jenna Houle<sup>1</sup> and Kate Rossner<sup>#</sup>

<sup>1</sup>Santa Clara High School, Santa Clara, CA, USA

<sup>#</sup>Advisor

## ABSTRACT

Atherosclerotic cardiovascular disease (atherosclerosis) is the leading cause of death worldwide. While atherogenesis is generally well understood, the sustained inflammation seen in some rapidly developing plaques remains largely unexplained. Recent research in epigenetics reports chromatin remodeling with significant pro-atherogenic effects in human monocytes exposed to oxLDL. Data collected from isolated monocytes *in vitro* suggests that epigenetic innate immune training may explain the observed persistent inflammatory state, however, research has yet to quantify the effects of training on early plaque dynamics. In the present study, I employ a partial differential equation and agent based mathematical model to describe key markers of atherogenesis in a system with “untrained” or “trained” monocytes. Time dependent solutions of the model suggest that innate immune training with oxLDL produces a pronounced pro-inflammatory response which has significant effects on the counts of plaque macrophages and foam cells. These results provide further support for the targeting of the epigenome in the treatment of atherosclerosis.

## 1 Introduction

### 1.1 Atherosclerosis

Atherosclerosis, or atherosclerotic cardiovascular disease (ASCVD), is a chronic inflammatory disease of the arteries responsible for the majority of heart attacks and strokes. As a result, ASCVD is the underlying cause of 50% of deaths in the Western world and the leading cause of death worldwide [1,2]. The disease develops through several stages beginning with the accumulation of immune cells within the intima\* [1,2,3,4].

**Table 1.** Nonstandard terminology. Terms are marked (\*) in text.

Term	Definition
<b>Endothelium:</b>	Layer of cells coating the inside of an artery, part of the intima
<b>Intima:</b>	Innermost layer of an artery
<b>LDL, HDL, OxLDL:</b>	Low density lipoprotein, high density lipoprotein, oxidized / modified LDL
<b>Reactive oxygen species:</b>	Highly reactive and unstable molecules containing oxygen, free radicals
<b>Monocyte:</b>	Circulating innate immune cell, macrophage progenitor
<b>Macrophage:</b>	Differentiated innate immune cell
<b>Cytokine:</b>	Class of small proteins released in cell signaling
<b>Chemoattractant:</b>	Molecules which attract motile cells
<b>M-CSF:</b>	Macrophage-colony stimulating factor, cytokine, induces monocyte differentiation
<b>Scavenger receptors:</b>	Class of cell surface receptors which bind lipid ligands

### 1.2 Early atherogenesis

Atherogenesis begins with damage to the endothelium\* caused by non-laminar, turbulent blood flow at areas of arterial curvature or bifurcation [1,2,3,5] (Supplemental Figure 2). Following endothelial damage, LDL\* cholesterol in the bloodstream diffuses into the intima\* where it is modified by reactive oxygen species\* released by damaged endothelial cells [1,3]. Modified LDL (oxLDL\*) is inflammatory and causes the remaining endothelial cells to produce cytokines\*, chemoattractants\*, and cell adhesion molecules which allow monocytes\* in the bloodstream to attach to the endothelium (Figure 2A at center) [2,3] and migrate into the intima. Once in the intima, M-CSF\* induces differentiation into macrophages\* (Figure 2A at center) [2,3]. These macrophages express proteins called scavenger receptors\* which recognize and internalize the lipid content of oxLDL [4,6,7]. Stimulated by this consumption, macrophages secrete chemoattractants and endothelial-stimulating (ES) cytokines which results in the recruitment of additional monocytes [4,7]. Macrophages which ingest a significant amount of oxLDL become large and immotile “foam cells” [2,4]. As ASCVD progresses, foam cells accumulate in the intima and form the early plaque (Figure 2A at right).

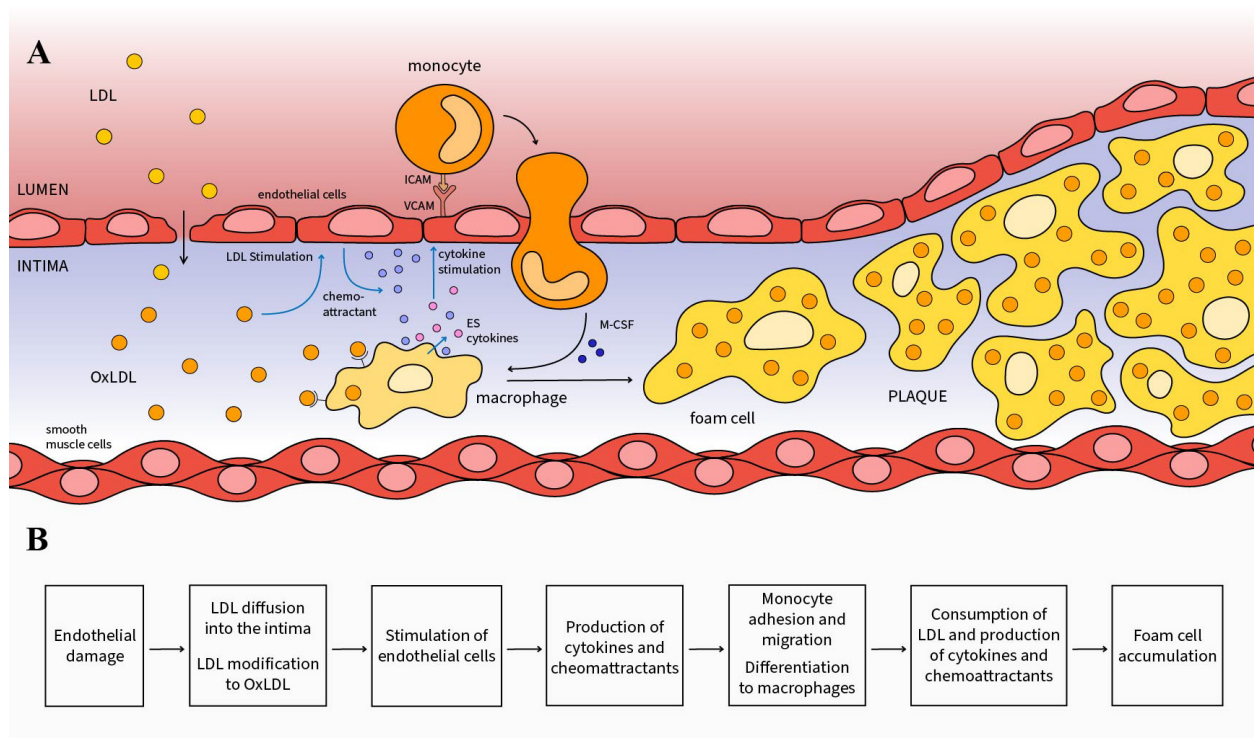
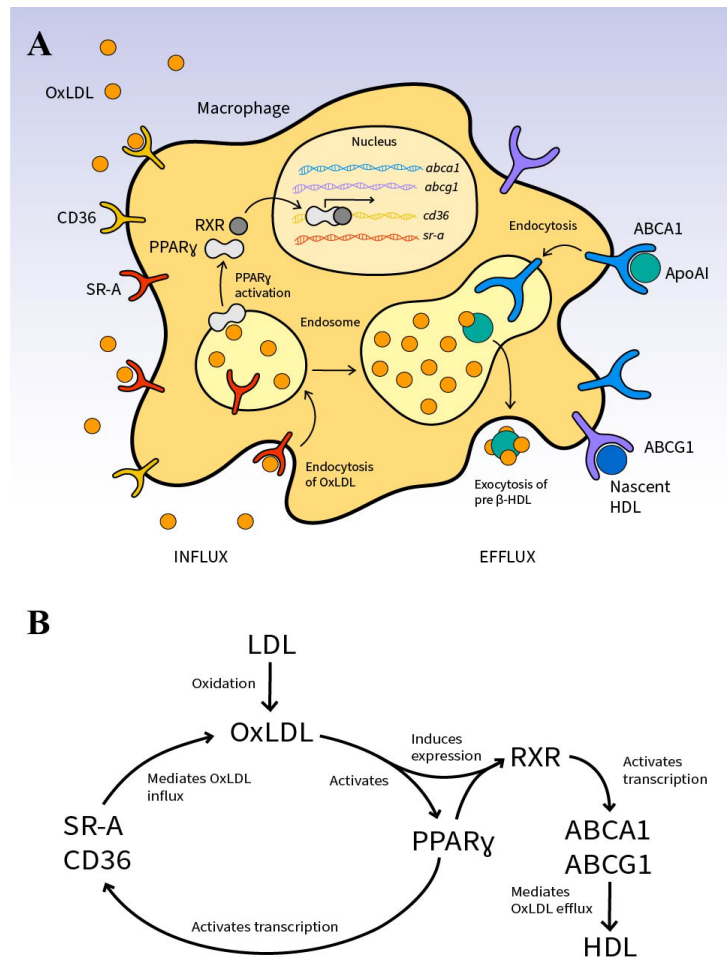


**Figure 2.** Graphic (A) and schematic (B) representations of early plaque formation. Left to right: LDL entry to the intima, stimulation of the endothelium, migration of monocytes, oxLDL consumption by macrophages, and accumulation of foam cells. Figure 2A adapted from Chalmers et al., 2015 [3].

### 1.3 Macrophages and oxLDL

Macrophages consume and process oxLDL as part of reverse cholesterol transport, a process where excess cholesterol is removed from peripheral tissues and transported to the liver [4]. Cholesterol influx transporters, including scavenger receptors SR-A and CD36, transport oxLDL into the macrophage where cholesterol content is stored in endosomes [4,8,9,10]. Macrophages also express cholesterol efflux transporters including ABCA1 and ABCG1 which bind and internalize lipid poor cholesterol acceptors including ApoAI and nascent HDL\* found in the bloodstream (Figure 3A) [4,11]. The acceptors are then lipidated by internalized cholesterol and exocytosed as pre-β or nascent HDL which travels through the bloodstream to the liver for further processing (Figure 3A) [4,11].

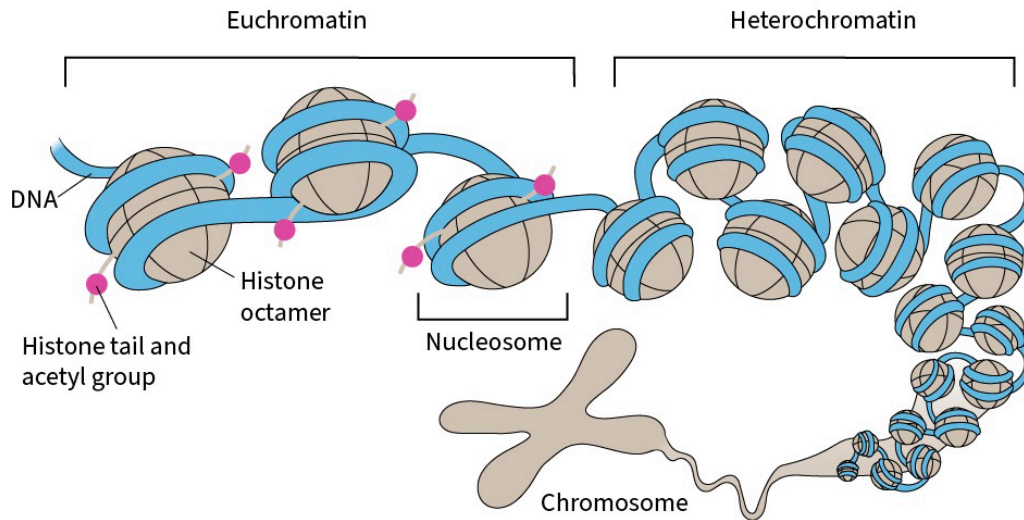
Importantly, both influx and efflux are up-regulated by oxLDL in a dose dependent manner via activation of the transcription factor PPAR $\gamma$  [7,12,13,14]. When PPAR $\gamma$  binds internalized oxLDL, it takes on an activated confor-



mation, associates with the RXR receptor, and moves to the nucleus [7,12]. The activated PPAR $\gamma$ -RXR complex then binds to the promoters of the *sr-a*, *cd36*, *abca1*, and *abcg1* genes where it up-regulates their transcription and subsequent expression [7,12]. At high oxLDL concentrations (~50  $\mu\text{g/ml}$ ), expression of all four transporters is increased ~2-4 fold [7]. At all concentrations, influx occurs faster than efflux resulting in net cholesterol influx and foam cell formation [7,11,12]. However, the rapid accumulation of cholesterol seen in atherosclerotic plaque macrophages exceeds the net influx expected from these mechanisms alone [15]. Recently, Bekkering, Christ, and others have presented evidence for epigenetic innate immune training by oxLDL which may explain this rapid growth [15,16,17,18].

**Figure 3.** Graphic (A) and schematic (B) representations of macrophage cholesterol influx and efflux via SR-A and CD36 and ABCA1 and ABCG1 respectively. Expression of all four transporters is up-regulated by oxLDL induced PPAR $\gamma$  activation creating a positive feedback loop (B). Figure 3B adapted from Chawla et al., 2001 [12].

#### 1.4 Epigenetic innate immune training by oxLDL



Immunity in vertebrates is achieved through two distinct but collaborative systems: the innate system and the adaptive system. Innate immune cells (including monocytes and macrophages) respond quickly to common pathogenic structures and provide initial recognition of pathogens. Adaptive immune cells (including B and T cells) create a stronger, more targeted response via antibody production but take ~14 days to do so [19,20]. Importantly, the adaptive system creates a “memory” of specific pathogens which expedites responses to the pathogen upon future exposure [19,20]. However, recent work in epigenetics has shown that innate cells can also produce a learned or “trained” response [21,22].

Cells can regulate their gene expression by making genetic material accessible or inaccessible for transcription through a process known as chromatin remodeling [23]. Chromatin state (heterochromatin or euchromatin) is driven by chemical residues added to histones tails or to DNA collectively referred to as epigenetic marks and the epigenome (Figure 4) [23]. While bases in the genome remain static, the epigenome undergoes constant remodeling in response to a variety of environmental stimuli [23].

**Figure 4.** Densely (heterochromatin) and loosely (euchromatin) packed DNA-histone complexes (nucleosomes).

Importantly, it has now been shown that exposure to oxLDL induces genome-wide epigenetic modification and marked phenotype changes in innate immune cells (referred to as epigenetic innate immune training) [15,16,17,18,24,25]. Bekkering et al. recently reported that cells incubated with low dose oxLDL showed an increase of activating epigenetic marks at the promoter regions of pro-atherogenic genes *tnfa*, *il-6*, *il-8*, *mcp-1*, *mmp2*, *mmp9*, *cd36*, and *sr-a* (Table 2) [15]. Training with oxLDL was also found to enhance foam cell formation through a significant up-regulation of SR-A and CD36 and down-regulation of ABCA1 and ABCG1 (Table 2) [15].

**Table 2.** Changes to gene regulation in oxLDL trained monocytes as reported by Bekkering et al. [15].

Response Type	Marker	Marker Description
Upregulation	IL-6, IL-8, IL-18	Interleukins 6, 8, and 18, inflammatory cytokines
	TNF $\alpha$	Tumor necrosis factor $\alpha$ , inflammatory cytokine
	MCP-1	Monocyte chemoattractant protein 1
	SR-A, CD36	Macrophage scavenger receptors
	MMP2, MMP9	Matrix metalloproteinases 2 and 9, plaque destabilizers
Downregulation	ABCA1, ABCG1	Cholesterol efflux transport proteins

### 1.5 Study objectives

These trained changes to monocyte behavior have clear implications for atherosclerosis; increased production of inflammatory cytokines and chemoattractants paired with changes in cholesterol transporter regulation are very likely pro-inflammatory and pro-atherogenic [15,26]. Though these phenomena have been explored with isolated monocytes, research has yet to quantify the effects of oxLDL induced epigenetic training on the entire early plaque. In this work, I aim to use a partial differential equation and agent based model to describe the effect of this epigenetic training on intimal oxLDL concentration, intimal cytokine concentration, monocyte migration rate, intimal macrophage count, oxLDL consumption rate, and intimal foam cell count. This work aims to address three gaps in the literature: an incomplete understanding of rapidly developing atherosclerotic plaques, an incomplete understanding of how epigenetic training of monocytes impacts the plaque environment, and a lack of modeling tools considering training.

## 1.6 Mathematical models of atherosclerosis

Atherosclerosis is intrinsically difficult to study; poor measurement instruments and ethical constraints limit study *in vivo* and the complexity of the plaque environment limits study *in vitro* [1,3,27]. In response, groups have begun to use modeling *in silico* (mathematical or computer simulations) to represent and make predictions about atherogenesis [27]. Many such models exist, with focus on all stages of ASCVD ranging from blood flow and endothelial damage to early plaque dynamics, to late stage hardening, necrosis, and destabilization [3,27-32]. Accordingly, these models take different approaches, but are typically multivariable functions of time and space [3]. In this work, I adapt a model presented by Chalmers et al. in 2015 and consider the concentrations of five agents (oxLDL, cytokines, chemoattractant, macrophages, and foam cells) as they vary with time and one-dimensional space. This model considers plaque dynamics during the first 30 days of atherogenesis when the epigenetic changes of interest are most relevant. Like most other models of atherosclerosis, the present model is qualitative and based on estimates of relative concentrations and rates [3,27].

## 2 Development of the model

### 2.1 Approach

In this Section I will introduce a set of partial differential equations (PDEs) which describe the dynamics of early atherosclerotic plaques discussed in Section 1. These equations are adapted from the model presented by Chalmers et al. in 2015 (subsequently referred to as “the Chalmers model”) [3]. For this study, I chose to adapt an existing model because previous works have established a description of dynamics in early plaques which is unchanged by training. I specifically selected the Chalmers model because it considers the agents relevant to training over the time period of interest (early atherogenesis). A full review of the Chalmers model is available in the Supplement (Section S.1); thus, the following subsections will focus on the novel features of the present model: the addition and quantification of efflux, the quantification of influx, and the modification of terms to represent oxLDL induced epigenetic training. Through these features, this model provides a framework for studying the effects of trained innate immunity (subsequently referred to as “training”) on several key markers of atherogenesis. As previously described, the model consists of equations for the following quantities:

$l(x, t)$	Concentration of oxLDL	$m(x, t)$	Count of intimal macrophages
$a(x, t)$	Concentration of chemoattractants	$f(x, t)$	Count of intimal foam cells
$c(x, t)$	Concentration of ES cytokines		

where each quantity is a function of position  $x$  and time  $t$ . The model operates under the same assumptions of initial conditions made by the Chalmers model and uses the same definition of position  $x$  and boundary conditions because the initial state and behaviors of the artery wall are unchanged by training (Section S.1) [15].

## 2.2 OxLDL (l)

The concentration of intimal oxLDL is modeled by:

$$\frac{\partial l}{\partial t} = D_l \frac{\partial^2 l}{\partial x^2} - I - d_l l$$

Diffusion and decay (the first and third terms respectively) were maintained from the Chalmers model because training has no effect on these processes (diffusion and decay will be rescaled to fit the timescale of this model in Section 3). Cholesterol consumption was replaced with an influx term  $I$  which relates cholesterol consumption to influx transporter expression. Influx  $I$  will be defined in Sections 2.6-2.9.

## 2.3 Chemoattractants (a) and ES cytokines (c)

The concentration of intimal chemoattractants and endothelial-stimulating cytokines are modeled by:

$$\frac{\partial a}{\partial t} = D_a \frac{\partial^2 a}{\partial x^2} + \mu_a E_a(I) - d_a a \quad \text{and} \quad \frac{\partial c}{\partial t} = D_c \frac{\partial^2 c}{\partial x^2} + \mu_c E_c(I) - d_c c$$

respectively. The diffusion and decay terms were maintained from the Chalmers model but will be rescaled. Cholesterol consumption was again replaced with influx  $I$ . An additional constant,  $E_a$  or  $E_c$  (relative expression of chemoattractant and cytokine genes respectively) was added to each equation to account for differences in gene expression in trained and untrained macrophages [15].  $E_a$  and  $E_c$  will be defined in Section 3.

## 2.4 Monocytes / macrophages (m)

The count of intimal macrophages is modeled by:

$$\frac{\partial m}{\partial t} = D_m \frac{\partial^2 m}{\partial x^2} - X_m \frac{\partial}{\partial x} \left( m \frac{\partial l}{\partial x} \right) - \frac{\partial f}{\partial t} - d_m m$$

The diffusion, chemotaxis, and decay terms were maintained from the Chalmers model. Cholesterol consumption was replaced with the PDE for foam cells (2nd from right) which includes cholesterol efflux for improved accuracy.

## 2.5 Foam cells (f)

The count of intimal foam cells is modeled by:

$$\frac{\partial f}{\partial t} = \mu_f (I - E)$$

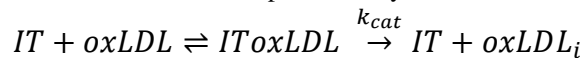
Macrophages are designated foam cells based on high internal cholesterol content [4], so foam cell formation rate was taken as proportional to the rate of change of cholesterol content. In plaque macrophages, this rate is a net influx [4] defined by influx  $I$  minus efflux  $E$ . Importantly, this equation considers cholesterol removed via efflux transporters while the Chalmers model did not.

## 2.6 Michaelis-Menten kinetics in influx and efflux

As discussed in Section 1.4, oxLDL training has a significant impact on the expression of cholesterol influx and efflux transporters, neither of which are included explicitly in the Chalmers model (Section S.1). Thus, the following sections will describe the derivation of influx and efflux terms based on transporter expression. Influx rate varies with receptor expression and oxLDL concentration. At low oxLDL concentrations, influx rate is limited by oxLDL availability and is approximately linear to oxLDL concentration [3,33,34]. This remains true until oxLDL concentration approaches a saturating concentration where influx rate is instead limited by SR-A and CD36 receptor expression [3,33,34]. This description follows Michaelis-Menten type kinetics which models enzyme mediated reactions of the form:



where  $E$  represents the enzyme and  $S$  represents the substrate [33,34]. When enzyme and substrate are present, they bind to form an enzyme-substrate complex  $ES$  which can dissolve back into reactants or react irreversibly to produce a new product  $P$  and unmodified free enzyme  $E$  at a rate of  $k_{cat}$  reactions per unit of time [33,34]. Though cholesterol influx is not an enzyme mediated reaction, the processes share similar dynamics and Michaelis-Menten type kinetics can be applied [3,32]. Here, cholesterol influx can be represented by:



where influx transporters ( $IT$ ) SR-A and CD36 act as the “enzyme” and oxLDL acts as the substrate. When oxLDL binds SR-A or CD36, a transporter-substrate complex is formed. OxLDL can then unbind to dissolve the complex or the two can be endocytosed at a rate of  $k_{cat}$  to yield free SR-A or CD36 and internalized cholesterol (Section 1.3). Similarly, cholesterol efflux can be represented by:

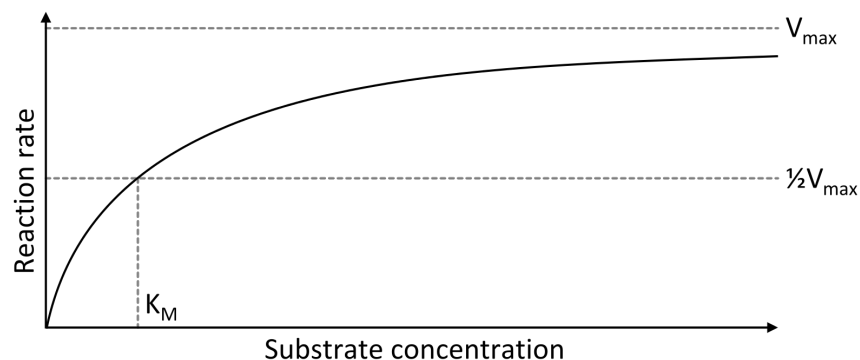


where efflux transporters ( $ET$ ) ABCA1 and ABCG1 act as the “enzyme” and both cholesterol acceptors ( $A$ ) and internal oxLDL ( $oxLDL_i$ ) act as substrates. In this model, I take acceptor concentration as greater than saturating concentration and therefore as non-rate-limiting. This assumption is based on data from Geeraert et al. which shows blood-stream concentrations of ApoAI and HDL 10 times the saturating concentration in pigs [8]. The transporter-acceptor-oxLDL complex is then exocytosed as a rate of  $k_{cat}$  to yield free ABCA1 or ABCG1 and lipidated cholesterol acceptors ( $A_l$ ).

The rate of a Michaelis-Menten type processes is given by the general form:

$$V = \frac{V_{max}[S]}{K_m + [S]} \quad V_{max} = k_{cat} [E]$$

where  $V$  represents the reaction velocity,  $V_{max}$  represents the maximum rate of the reaction,  $[S]$  represents substrate concentration,  $[E]$  represents enzyme or receptor concentration,  $k_{cat}$  represents the efficiency of the enzyme or recep-



tor, and  $K_m$  represents the  $[S]$  at which  $V = 1/2V_{max}$  (Figure 5) [33,34].

**Figure 5.** Reaction rate vs substrate concentration for a Michaelis-Menten type reaction. Image from Shafee [36].

For cholesterol influx, the reaction velocity  $I$  (for a single macrophage) is:

$$I = \frac{V_{max} l}{K_m + l} \quad V_{max} = k_{cat} i [IT]$$

where the substrate concentration  $l$  is [oxLDL] and the “enzyme” concentration  $[IT]$  is the concentration of influx transporters SR-A and CD36 present. As described previously (Section 1.3), influx transporter expression varies with PPAR $\gamma$  regulation. Thus,  $V_{max}$  for influx is better described by:

$$V_{max} = k_{cat} i [IT_{base}] E_i$$

where  $[IT_{base}]$  is the concentration of influx transporters at some base expression and  $E_i$  is the relative expression following PPAR $\gamma$  regulation ( $E_i = 1$  at base expression).

Though accurate, this is an impractical description because receptor expression is not typically measured as a concentration.  $V_{max}$  can instead be given by:

$$V_{max} = Eff_{base} i E_i$$

where  $Eff_{base} i$  is the efficiency of influx via SR-A and CD36 (in % per 6 hours) at base transporter expression ( $E_i = 1$ ). Efflux transporter expression is also regulated by PPAR $\gamma$ , so influx and efflux rate are given by:

$$I = \frac{Eff_{base} i E_i l}{K_m + l} \quad E = \frac{Eff_{base} e E_e l}{K_m + l}$$

which can be further simplified to give:

$$I = \frac{Eff_{base} i E_i l}{1.0 + l} \quad E = \frac{Eff_{base} e E_e l}{1.0 + l}$$

where 1 is used for  $K_m$  because of a lack of data for receptor specific components of influx and efflux. This substitution is used in other models and has a minimal effect on accuracy [3,32]. In the efflux equation, internal oxLDL is replaced with intimal oxLDL because it is beyond the scope of this model to consider individual macrophage cholesterol content.

## 2.7 Relative expression of influx and efflux transporters

PPAR $\gamma$  activation varies with ligand concentration ([oxLDL]) in a dose dependent manner [7,12,14]. Nagy showed increased expression (~4 fold maximum) of a manufactured reporter gene with PPAR $\gamma$  sites in the promoter when exposed to 0, 1, 10, and 50  $\mu\text{g/ml}$  of oxLDL [7]. I plotted this data and performed a regression which revealed that PPAR $\gamma$  regulation can be described by a natural log (ln) function (Figure 6). Data by Chinetti confirms that a natural log function is a good descriptor of PPAR $\gamma$  up-regulation [14].

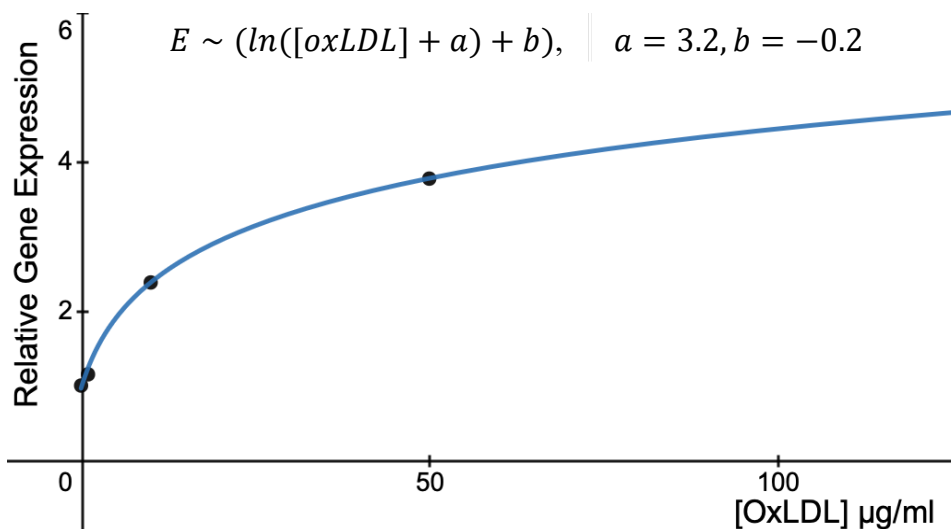


**Figure 6.** Relative (fold) expression of a reporter gene at varying oxLDL concentrations. Points represent data from Nagy et al., curve represents an expression function achieved through regression conducted with the Desmos graphing calculator [7].

However, data by Nagy, Chalwala, and Chinetti show that influx and efflux transporters are not up-regulated to a uniform level of relative expression [7,12,14]. Instead, influx transporters SR-A and CD36 are up-regulated less strongly than efflux transporters ABCA1 and ABCG1 [7,14]. Using data for CD36 expression [7] at 0 and 50  $\mu\text{g/ml}$  oxLDL (no exposure and high dose), I performed a second regression yielding a function of influx transporter expression (Figure 7).

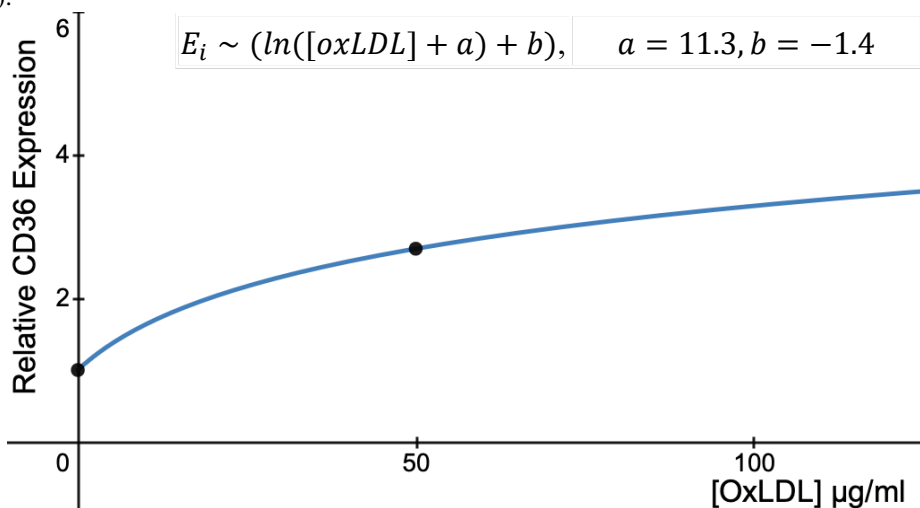


**Figure 7.** Relative expression of CD36 versus oxLDL concentration. Points represent data from Nagy et al., curve represents expression function achieved through regression.

Nagy observed that CD36 and SR-A up-regulation were of similar magnitude via western blot [7], thus, I take the total relative expression of influx transporters to be:

$$E_i = \ln(l + 11.3) - 1.4$$

where  $l$  is [oxLDL]. Data from Chinetti shows  $\sim 4$  fold up-regulation of ABCA1 in the presence of high dose rosiglitazone (a PPAR $\gamma$  ligand). Because this is similar to the up-regulation observed by Nagy in their reporter gene (Figure 6) and because ABCA1 and ABCG1 are similarly up-regulated by PPAR $\gamma$  [12], I take the total relative expression of efflux transporters to be:

$$E_e = \ln(l + 3.2) - 0.2$$

## 2.8 Base efficiency of influx and efflux transporters

The above models of influx and efflux transporter expression can be used to solve for base receptor efficiency ( $Eff_{base\ i}$ ,  $Eff_{base\ e}$ ). In cells expressing only ABCA1, Chinetti reported  $\sim 10\%$  efflux per 6 hours at very low dose oxLDL and Yvan-Charvet reported  $\sim 40\%$  cholesterol efflux per 6 hours at high dose oxLDL [9,14]. In cells expressing only ABCG1, Gelissen reported  $\sim 8\%$  efflux per 6 hours at very low concentrations of nascent HDL (the cholesterol acceptor for ABCG1) and  $\sim 30\%$  efflux per 6 hours at high concentrations of nascent HDL [11]. Because ABCA1 and ABCG1 act on different cholesterol acceptors, and are therefore non-competitive, I assume efflux via these transporters is additive. This assumption gives  $\sim 18\%$  efflux per 6 hours at very low dose oxLDL and  $\sim 70\%$  efflux per 6 hours at high dose oxLDL. Using these values and the equation for efflux presented in Section 2.6, I performed a regression to solve for base efflux efficiency  $Eff_{base\ e}$  (Figure 8).

Cholesterol influx is not commonly measured or reported alone, thus, I used net influx data and the efflux model developed above to solve for the base efficiency of influx transporters. Bekkering reported net influx as ~40 pg/ml ApoB (apolipoprotein B, a protein component of oxLDL) at very low dose oxLDL and ~50 pg/ml ApoB at high dose oxLDL [15]. It's important to note that this net influx is not solely the result of the four influx and efflux transporters considered here. Nicholson reports that ~25% of cholesterol influx is non CD36 or SR-A specific [6] and Yvan-Charvet reports that ~15% of efflux is non ABCA1 or ABCG1 specific [9]. Based on this data, I take 10% of net influx as nonspecific (4 pg/ml at low oxLDL, 5 pg/ml at high oxLDL). These ApoB concentrations do not directly correspond to oxLDL content of a single macrophage, so values were standardized to give relative net influx of 1 at very low dose oxLDL and 1.25 at high dose oxLDL (Table 3).

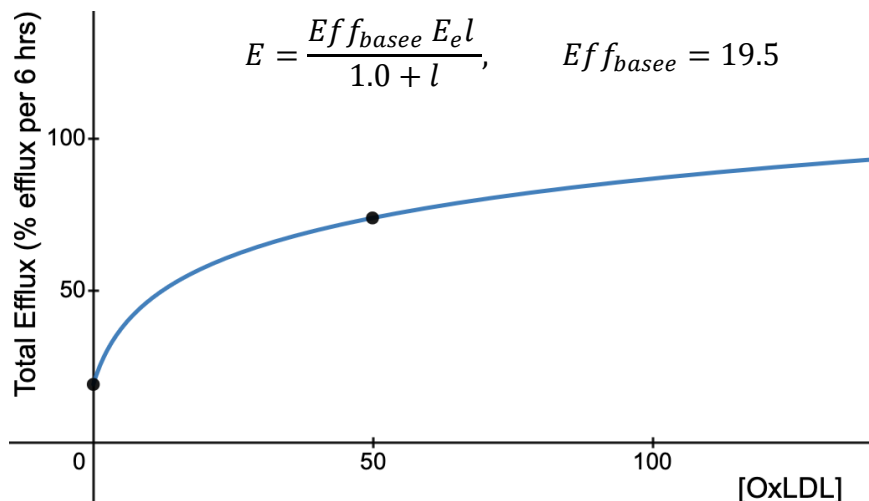


**Figure 8.** ABCA1 and ABCG1 mediated (total) efflux rate versus oxLDL concentration. Points represent data from Chinetti et al. and Yvan-Charvet et al. [9,14], curve represents efflux function with fit value of  $Eff_{base\ e}$  achieved through regression.

**Table 3.** Net influx at very low and high dose oxLDL in untrained macrophages.

Untrained	Reported net influx	Specific net influx	Standardized net influx
2 µg/ml oxLDL	40 pg/ml ApoB	40(0.9) = 36 pg/ml	1
50 µg/ml oxLDL	50 pg/ml ApoB	50(0.9) = 45 pg/ml	1.25

Net influx can be described as influx - efflux ( $I - E = N$ ) giving:

$$\frac{Eff_{base\ i} E_i l}{1.0 + l} - \frac{Eff_{base\ e} E_e l}{1.0 + l} = 1 \quad [l = 2]$$

$$\frac{Eff_{base\ i} E_i l}{1.0 + l} - \frac{Eff_{base\ e} E_e l}{1.0 + l} = 1.25 \quad [l = 50]$$

where  $l$  is the concentration of oxLDL. Filling in previously described values for  $Eff_{base\ e}$ ,  $E_e$ ,  $E_i$ , and  $l$  gives:

$$Eff_{base\ i}(0.79) - 18.83 = 1$$

$$Eff_{base\ i}(2.66) - 72.15 = 1.25$$

$Eff_{base\ i}$  cannot be calculated from relative net influx directly because of mismatched units. Thus, rescaling the second equation and equating the two equations gives: (where  $Eff_{base\ i}$  is in units of % influx per 6 hours)

$$Eff_{base\ i}(0.79) - 18.83 = 1, Eff_{base\ i}(2.13) - 57.72 = 1$$

$$Eff_{base\ i}(0.79) - 18.83 = Eff_{base\ i}(2.13) - 57.72$$

$$Eff_{base\ i} = 29.07$$

## 2.9 Expression of transporters following training

As discussed in Section 1.4, expression of influx and efflux transporters are increased and decreased respectively following training [15]. These changes to expression are reflected in trained versions of the relative expression terms,  $E_i$  and  $E_e$ . Following training, the PPAR $\gamma$  pathway continues to up-regulate the expression of influx and efflux transporters in the presence of oxLDL, however, the epigenetic marks characteristic of training alter the magnitude of expression achieved [15].

Bekkering reported net influx following training as ~40 pg/ml ApoB at very low dose oxLDL and ~150 pg/ml ApoB at high dose oxLDL [15]. I again consider nonspecific influx and efflux but assume that the rate of nonspecific net influx remains 4 pg/ml/6hrs at low oxLDL and 5 pg/ml/6hrs at high oxLDL because training likely has no effect on nonspecific net influx. Values were then standardized to relative net influx of 1 and 4 (Table 4). Using the values of base efficiency defined previously, I calculated the net influx (in % per 6 hours) of untrained macrophages exposed to 2 and 50  $\mu$ g/ml oxLDL. I then calculated the net influx for trained macrophages using the standardized values presented above (Table 5).

**Table 4.** Net influx at very low and high dose oxLDL in trained macrophages.

Trained	Reported net influx	Specific net influx	Standardized net influx
2 $\mu$ g/ml oxLDL	40 pg/ml ApoB	40 - 4 = 36 pg/ml	1
50 $\mu$ g/ml oxLDL	150 pg/ml ApoB	150 - 5 = 145 pg/ml	4

**Table 5.** Net influx (in % per 6 hours) for untrained and trained macrophages at very low and high [oxLDL] ( $l$ ).

	[oxLDL]	$(E_i)\left(\frac{Eff_{basei}l}{1.0+l}\right) - (E_e)\left(\frac{Eff_{basee}l}{1.0+l}\right) = N$	Standardized net influx
Untrained	2	$(1.19)(19.38) - (1.45)(13.00) = 4.19\%$	1
	50	$(2.72)(28.50) - (3.77)(19.12) = 5.25\%$	1.25
Trained	2	$(E_{i\text{ trained}})(19.38) - (E_{e\text{ trained}})(13.00) = \mathbf{4.19\%}^1$	1
	50	$(E_{i\text{ trained}})(28.50) - (E_{e\text{ trained}})(19.12) = \mathbf{16.87\%}$	4

<sup>1</sup> Bolded values for trained macrophages were derived from standardized values of net influx.

At very low [oxLDL], net influx is constant (~4% per 6 hours) regardless of training. Therefore, at  $l = 2$ , the relative expression of transporters is the same for untrained and trained macrophages, giving:

$$E_{i\text{ trained}} = E_i = 1.19, E_{e\text{ trained}} = E_e = 1.45 [l = 2]$$

Bekkering reports an ~5 fold increase in CD36 and SR-A and an ~4 fold decrease in ABCA1 and ABCG1 following training and TLR 2 stimulation (exposure to a non-oxLDL ligand) [15]. These results do not directly correspond to up-regulation via oxLDL stimulation [36], so values were standardized to +1 and -0.8. Thus, net influx in trained macrophages exposed to 50  $\mu$ g/ml oxLDL can be represented by:

$$\begin{aligned} (E_{i\text{ trained}})(28.50) - (E_{e\text{ trained}})(19.12) &= 16.87\% \\ (E_i + 1n)(28.50) - (E_e - 0.8n)(19.12) &= 16.87\% \end{aligned}$$

Which gives:

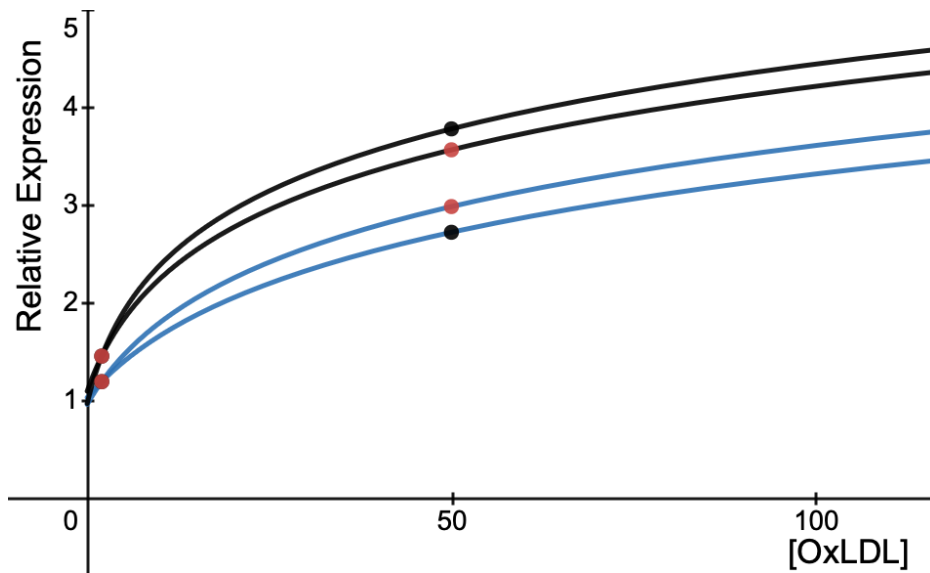
$$n = 0.264$$

$$E_{i\text{ trained}} = 2.98, E_{e\text{ trained}} = 3.56 [l = 50]$$

I then plotted the  $E_{i\text{ trained}}$  and  $E_{e\text{ trained}}$  values for high and low oxLDL and performed a regression which gave the following functions:

$$E_{i\text{ trained}} = \ln(l + 7.6) - 1.1 \quad \text{and} \quad E_{e\text{ trained}} = \ln(l + 4.6) - 0.4$$

The relative expression of influx and efflux transporters in trained and untrained macrophages is summarized in Figure



9.

**Figure 9.** Relative expression of influx (blue curves) and efflux (black curves) transporters in trained (red points) and untrained (black points) macrophages vs [oxLDL]. Training increases influx transporter expression and decreases efflux transporter expression. Untrained curves for influx and efflux are shown in Figures 7 and 6 respectively. Function domains are limited to values of [oxLDL] > 0.

### 3 Model equations and constants

#### 3.1 Model equations

The five PDEs are:

$$\frac{\partial l}{\partial t} = D_l \frac{\partial^2 l}{\partial x^2} - I - d_l l \qquad \frac{\partial m}{\partial t} = D_m \frac{\partial^2 m}{\partial x^2} - X_m \frac{\partial}{\partial x} \left( m \frac{\partial l}{\partial x} \right) - \frac{\partial f}{\partial t} - d_m m$$

$$\frac{\partial a}{\partial t} = D_a \frac{\partial^2 a}{\partial x^2} + \mu_a E_a(I) - d_a a \qquad \frac{\partial f}{\partial t} = \mu_f(I - E)$$

$$\frac{\partial c}{\partial t} = D_c \frac{\partial^2 c}{\partial x^2} + \mu_c E_c(I) - d_c c$$

The equations for influx and efflux are:

$$I = m \frac{116.28E_i l}{1.0 + l}, \quad E = m \frac{78.00E_e l}{1.0 + l}$$

where base efficiency was rescaled from units of percent influx or efflux per 6 hours to percent influx or efflux per 24 hours (the time unit for the model) and the functions were multiplied by  $m$  (intimal macrophage count) to represent total influx and efflux.

The expression of influx and efflux transporters in untrained and trained macrophages is given by:

$$E_i = \ln(l + 11.3) - 1.4, E_{i \text{ trained}} = \ln(l + 7.6) - 1.1$$

$$E_e = \ln(l + 3.2) - 0.2, E_{e \text{ trained}} = \ln(l + 4.6) - 0.4$$

For boundary and initial conditions, see the Supplement (Section S1).

### 3.2 Equation constants

Many of the constants in this model are orders of magnitude approximations because they represent quantities which are unknown due to insufficient available data and measurement capabilities [3,27]. However, the values of  $D_l$ ,  $D_a$ ,  $D_c$ ,  $\mu_a$ ,  $\mu_c$ ,  $E_a$ , and  $E_c$  have been derived from experimental data. This model reflects a time unit of ~24 hours.

**Table 6.** Values of diffusion constants rescaled to time and space from experimental data like in the Chalmers model.  $D_m$  is taken to be much smaller than  $D_l$  because much larger macrophages diffuse more slowly than oxLDL.

Parameter	Raw value	Source	Rescaled value
$D_l$	$2.3 \mu\text{m}^2/\text{s}$	Dabagh et al. [3, 37]	$5.2 \times 10^1$
$D_a$	$\sim 100 \mu\text{m}^2/\text{s}$	Paavola et al. [3, 38]	$5.2 \times 10^1$
$D_c$	$\sim 100 \mu\text{m}^2/\text{s}$	Paavola et al. [3, 38]	$5.2 \times 10^1$
$D_m$	—	$D_m \ll D_l$	$5.2 \times 10^1$

**Table 7.** Values of decay constants ( $d_l, d_a, d_c, d_m$ ) are taken to be orders of magnitude smaller than the diffusion constants in Table 6. Values of  $\mu_a$  and  $\mu_c$  correspond to cytokine and chemoattractant production with respect to oxLDL consumption (~40 times more chemoattractant production than influx, ~10 times more chemoattractant production than cytokine production [15]).  $\mu_f$  is taken to be very small because a large amount of oxLDL must be consumed before a macrophage is considered a foam cell [3,4].

Parameter	Value	Parameter	Value
$d_l$	$5.0 \times 10^{-1}$	$\mu_a$	$4.0 \times 10^1$
$d_a$	$5.0 \times 10^{-1}$	$\mu_c$	$4.0 \times 10^0$
$d_c$	$5.0 \times 10^{-1}$	$\mu_f$	$4.0 \times 10^{-2}$
$d_m$	$5.0 \times 10^{-3}$		

**Table 8.** Values of additional model constants.  $X_m, \sigma_{a1}, \sigma_{a2}, \beta_a, \sigma_c$  are taken from the Chalmers model and are rescaled to 24 hour unit time [3].  $A_0$  and  $C_0$  represent bloodstream concentrations of chemoattractant and cytokines and are from the Chalmers model.  $E_a, E_c, E_{a \text{ trained}}, E_{c \text{ trained}}$  represent relative cytokine and chemoattractant gene expression in trained and untrained macrophages. Bekkering et al. report an ~4 fold increase in cytokine production and an ~3 fold increase in chemoattractant production in trained cells over untrained cells [15].

Parameter	Value	Parameter	Value	Parameter	Value
$X_m$	$5.0 \times 10^{-3}$	$\sigma_c$	$5.0 \times 10^{-3}$	$E_a$	1
$\sigma_{a1}$	$5.0 \times 10^2$	$A_0$	$1.0 \times 10^{-1}$	$E_c$	1
$\sigma_{a2}$	$5.0 \times 10^0$	$C_0$	$1.0 \times 10^{-2}$	$E_{a \text{ trained}}$	3
$\beta_a$	$1.0 \times 10^0$			$E_{c \text{ trained}}$	4

### 3.3 Solving the differential equations

I used the FlexPDE7 software package to calculate and display time dependent solutions of the given PDEs at different values of two parameters of interest:  $\sigma_l$  and  $\sigma_m$  which control the rate of LDL and monocyte entry into the intima respectively [3]. These parameters are of particular importance because  $\sigma_l$  is representative of blood LDL levels and

diet cholesterol and  $\sigma_m$  is representative of circulating monocyte counts associated with co-morbidities including diabetes mellitus and arthritis [2-4]. The FlexPDE7 code used is available in the Supplement (Section S.3).

## 4 Results

In Figures 10 and 11 I present results for several markers of atherogenesis in systems with untrained (at left) and trained (at right) macrophages at low (Figure 10) and high (Figure 11) blood LDL concentrations ( $\sigma_l$ ). Both oxLDL and chemoattractant concentration are maximized at the endothelium, so the plotted values at  $x = 0$  provide a good representation of their effects on the system (Figure 10A, B; Figure 11A, B; Supplemental Figure 1i, ii; Supplemental Figure 2i, ii) [3]. For all plots, each curve represents a solution at a different value of  $\sigma_m$ , which controls circulating monocyte levels.

Following epigenetic training, macrophages exhibit increased influx transporter expression, decreased efflux transporter expression, and increased cytokine and chemoattractant production (Section 1.4). In agreement with analysis by Bekkering, this model shows that these effects are pro-atherogenic [15].

### 4.1 Dynamics at low blood LDL

Figure 10 displays dynamics at a low blood LDL level consistent with a standard or low cholesterol diet. For all macrophages, the concentration of oxLDL at the endothelial boundary (Figure 10A, B) increases immediately following injury and then decreases as macrophages begin to infiltrate the intima and consume the cholesterol. At all circulating monocyte levels (all values of  $\sigma_m$ ), the concentration of oxLDL achieves a quasi-steady state after ~30 days. In systems with trained macrophages, the model reports less consumption of oxLDL (Figure 10B) in low monocyte cases (curves 1 (purple), 2 (blue)) and more consumption in high monocyte cases (curves 3 (yellow), 4 (orange)). As reported by Chalmers, there is an apparent switch between a low and high inflammatory state somewhere between  $\sigma_m = 4.0 \times 10^{-6}$  and  $\sigma_m = 7.0 \times 10^{-6}$  [3]. Macrophage training has very little effect on cytokine and chemoattractant production (Supplemental Figure 3i, ii) and monocyte migration (Supplemental Figure 3iii, iv) in low monocyte cases. However, in trained macrophages, increased cholesterol influx rate results in greater cholesterol accumulation and foam cell formation even at low values of  $\sigma_m$  (Figure 10F). Curves 1 and 2 represent atherogenesis limited by monocyte availability; though oxLDL at the boundary is high and endothelial cells produce chemoattractant, there are not enough monocytes in the bloodstream to respond, so the plaque grows slowly.

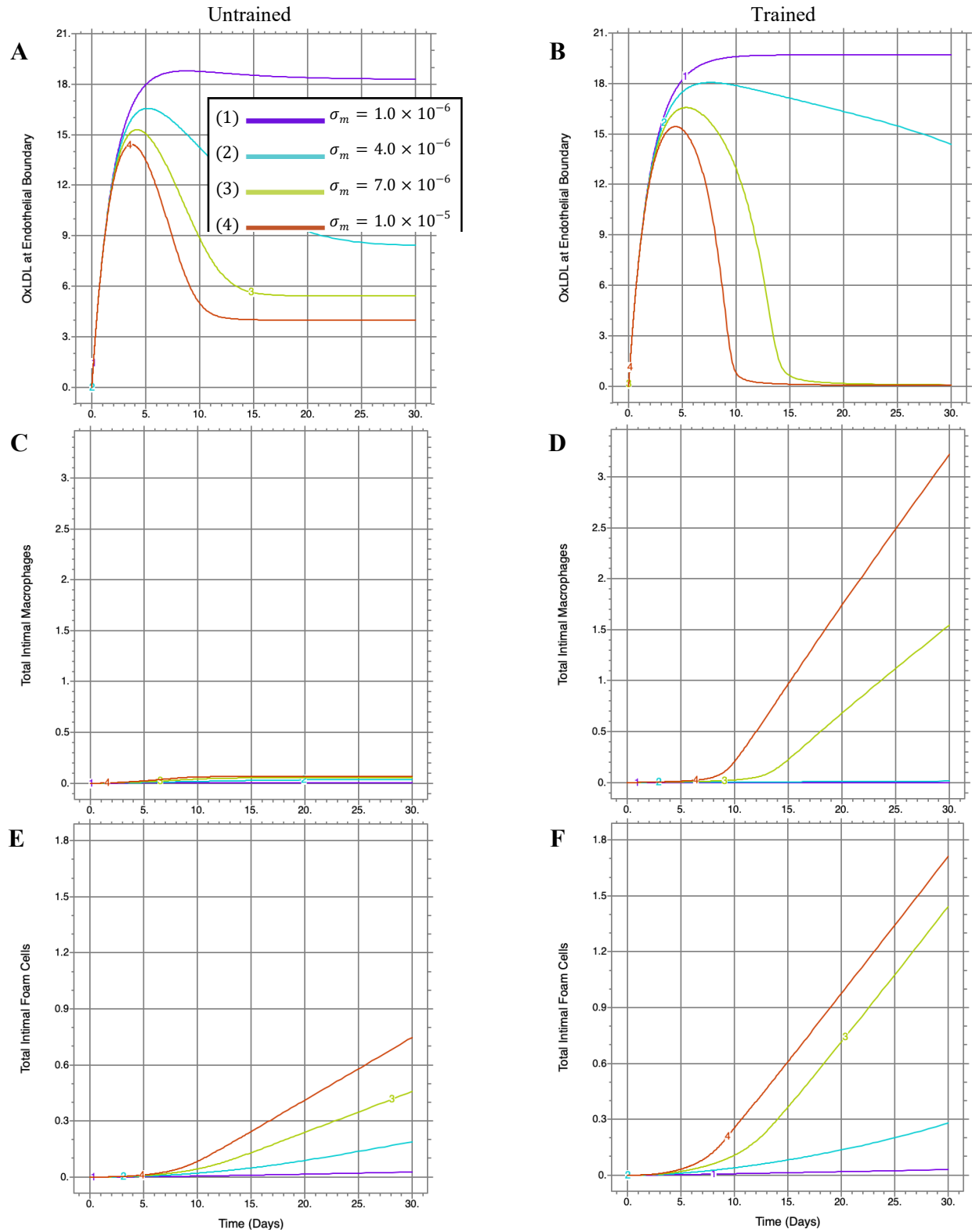


**Figure 10.** Model solutions at low LDL,  $\sigma_l = 1.0 \times 10^1$  at varying monocyte levels  $\sigma_m = 1.0 \times 10^{-6}$  to  $1.0 \times 10^{-5}$  (colored curves). (A), (B): concentration of oxLDL at the endothelial boundary  $l(0, t)$ ; (C), (D): total intimal macrophages (integral of  $m$ ); (E), (F): total intimal foam cells (integral of  $f$ ). All sets of plots use a time period of 30 days and display values for systems with untrained macrophages at left and trained macrophages at right.

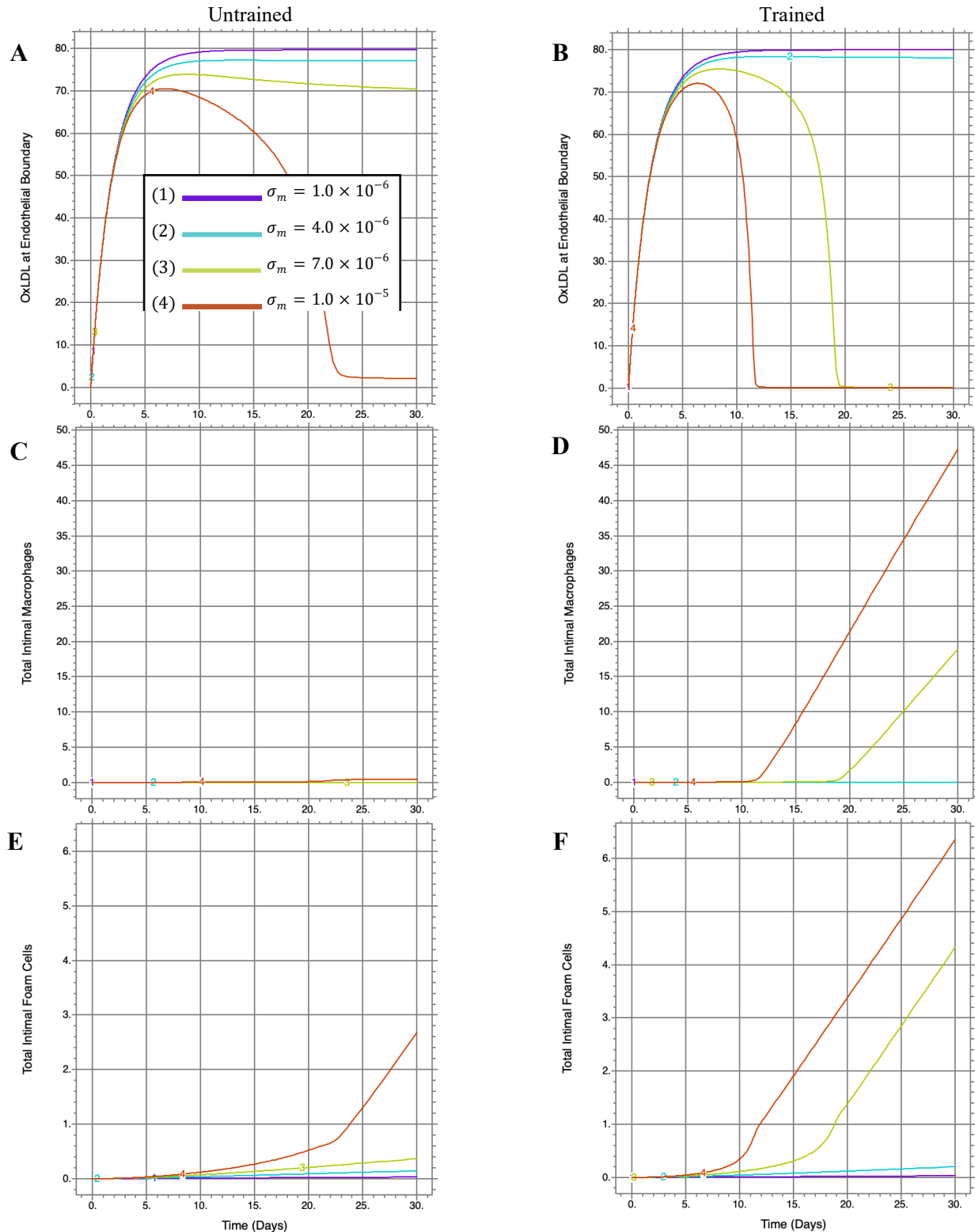


**Figure 11.** Model solutions at high LDL,  $\sigma_l = 4.0 \times 10^1$  at varying monocyte levels,  $\sigma_m = 1.0 \times 10^{-6}$  to  $1.0 \times 10^{-5}$  (colored curves). (A), (B): concentration of oxLDL at the endothelial boundary  $l(0, t)$ ; (C), (D): total intimal macrophages (integral of  $m$ ); (E), (F): total intimal foam cells (integral of  $f$ ). All sets of plots use a time period of 30 days and display values for systems with untrained macrophages at left and trained macrophages at right.

At high monocyte levels, the model considering training shows significantly decreased oxLDL concentrations (Figure 10B) at the boundary after 10-20 days which is explained by a significant increase in monocyte migration (Supplemental Figure 3iv). When a large number of monocytes are present in the bloodstream, more cells respond to the initial chemoattractant production by endothelial cells. As more monocytes migrate to the intima, the resulting trained macrophages produce a significantly increased number of chemoattractants and cytokines which further up-regulate monocyte recruitment. Importantly, curves 3 and 4 show a non-steady state for total intimal macrophages (Figure 10D) which indicates that the rate of monocyte migration exceeds the rate of foam cell formation leaving a significant number of macrophages in the plaque. For curves 3 and 4, the model displays a more than 100% increase in intimal foam cells by day 30 in systems with trained macrophages. Even in systems with low blood LDL, the model suggests that macrophage training is significantly pro-inflammatory especially when circulating monocyte levels are high.

## 4.2 Dynamics at high blood LDL

Figure 11 displays dynamics at a high blood LDL level consistent with a high cholesterol diet. In both trained and untrained systems, curves 1 and 2 show increasing oxLDL concentration at the endothelium until consumption reduces concentration to a quasi-steady state (Figure 11A, B). Because endothelial oxLDL concentration is significantly increased with this value of  $\sigma_l$  ( $\sim 70$   $\mu\text{g/ml}$  vs.  $\sim 15$   $\mu\text{g/ml}$ ), the consumption of oxLDL by intimal macrophages is less apparent in curves 1 and 2. The most prominent feature of the trained model is the apparent switch to a highly inflammatory state between  $\sigma_m = 4.0 \times 10^{-6}$  and  $\sigma_m = 7.0 \times 10^{-6}$ . In the trained model, curves 3 and 4 display a drop in oxLDL concentration to  $\sim 0$  (Figure 11B) and a significant increase in chemoattractant production and monocyte migration (Supplemental Figure 4ii, iv). As with the low blood cholesterol model, curves 3 and 4 display a highly non-steady state for total intimal macrophages indicating that monocyte recruitment rate far exceeds foam cell formation rate (which is limited by [oxLDL]) (Figure 4D). For the highest circulating monocyte level (Figure 11F, curve 4), the trained model shows a more than 100% increase in foam cell formation rate over the model without training and an  $\sim 1000\%$  increase over the model without training at low blood LDL (Figure 10E).

## 5 Discussion

The present study predicts that innate immune training has a pronounced pro-inflammatory effect on atherogenesis. These results suggest that the increased cytokine and chemoattractant production associated with training greatly increases monocyte influx and intimal macrophage counts in a cycle of positive reinforcement when circulating monocyte counts are high. Trained intimal macrophages then display increased influx rates and decreased efflux rates which results in more rapid foam cell and plaque formation. In late stage atherosclerosis, increased expression of matrix metalloproteinases (plaque destabilizers) associated with training may additionally contribute to acceleration of plaque degradation [15]. These effects may account for the persistent pro-inflammatory state observed in atherosclerosis patients [2,4,15,26] and the consideration of trained innate immunity here likely provides a more accurate representation of early atherogenesis than other models of similar scope.

### 5.1 Model strengths and weaknesses

To my knowledge, this model is the first of its kind to describe and approximately quantify the effects of oxLDL innate immune training on early atherosclerotic plaque dynamics. The model for influx and efflux is corroborated by experimental data from 7 independent studies [7,9-12,14,15]. The results for cytokine and chemoattractant production, oxLDL consumption rate, and foam cell formation rate match data presented by Bekkering and the overall trends for the untrained model match closely with results presented by Chalmers [3,15].

This model is by no means a complete representation of plaque dynamics. The descriptions of influx and efflux only consider transport of oxLDL by SR-A, CD36, ABCA1, and ABCG1 when in reality, there are many more transporters and ligands which contribute to these processes. Influx and efflux were described by simple Michaelis-Menten type kinetics under the assumption that ApoAI and nascent HDL (efflux transporter ligands) are present in saturating concentrations. This is a significant simplification of the involved processes [2]. Additionally, the efflux model uses intimal oxLDL concentrations instead of internal oxLDL for simplicity. Importantly, this model only partially considers the anti-inflammatory effects of HDL and does not include the movement of macrophages out of the intima which is thought to contribute to plaque recovery [28,32]. The scope of the model does not include blood flow, late stage plaque dynamics, or T cell activity. Finally, the model only considers scenarios in which all macrophages are either “untrained” or “trained” immediately from the time of injury when training is likely dose dependent and may be impacted by other ligands and stimulus via additional pathways.

## 5.2 Conclusions and implications

This model provides further support for the targeting of the epigenome in the treatment of atherosclerosis. The epigenetic changes responsible for the pro-inflammatory state of trained macrophages may be a better target for treatment than other traditional co-morbidities including high blood LDL and high circulating monocyte counts. As described in Figure 11, a person at high risk for atherosclerosis could see their plaque growth rate (foam cell formation rate) as much as halved by preventing training or reverting macrophages to an untrained state, a change equivalent to reducing LDL levels more than 75 percent. There are no currently marketed epigenetic drugs which target macrophages in this way, though this technology may soon be practical through the use of CRISPR dCas9 [15].

Epigenetic innate immune training and its effects on atherogenesis warrant further study. Future modeling efforts should work to further improve the accuracy of model constants through the use of additional experimental data as it becomes available. The clear next step for the modeling process presented here is the consideration of training as it may occur within the plaque. Where the present model assumed full training from the time of injury, a more complex model would consider the switch from the untrained to trained state as macrophages are exposed to oxLDL and other inflammatory agents in the intima.

## Acknowledgments

I would like to express my gratitude to my advisor Kate Rossner.

## References

1. Pahwa R. Atherosclerosis [Internet]. StatPearls [Internet]. U.S. National Library of Medicine; 2020. Available from: <https://www.ncbi.nlm.nih.gov/books/NBK507799/>
2. Hansson GK, Libby P. The immune response in atherosclerosis: a double-edged sword. *Nature reviews immunology*. 2006 Jul;6(7):508-19. doi:[10.1038/nri1882](https://doi.org/10.1038/nri1882)
3. Chalmers AD, Cohen A, Bursill CA, Myerscough MR. Bifurcation and dynamics in a mathematical model of early atherosclerosis. *Journal of mathematical biology*. 2015 Dec;71(6):1451-80. doi:[10.1007/s00285-015-0864-5](https://doi.org/10.1007/s00285-015-0864-5)

4. Yu XH, Fu YC, Zhang DW, Yin K, Tang CK. Foam cells in atherosclerosis. *Clinica chimica acta*. 2013 Sep 23;424:245-52. doi:[10.1016/j.cca.2013.06.006](https://doi.org/10.1016/j.cca.2013.06.006)
5. Dhawan SS, Avati Nanjundappa RP, Branch JR, Taylor WR, Quyyumi AA, Jo H, McDaniel MC, Suo J, Giddens D, Samady H. Shear stress and plaque development. Expert review of cardiovascular therapy. 2010 Apr 1;8(4):545-56. doi:[10.1586/erc.10.28](https://doi.org/10.1586/erc.10.28)
6. Nicholson AC, Frieda S, Pearce A, Silverstein RL. Oxidized LDL binds to CD36 on human monocyte-derived macrophages and transfected cell lines: evidence implicating the lipid moiety of the lipoprotein as the binding site. *Arteriosclerosis, thrombosis, and vascular biology*. 1995 Feb;15(2):269-75. doi:[10.1161/01.atv.15.2.269](https://doi.org/10.1161/01.atv.15.2.269)
7. Nagy L, Tontonoz P, Alvarez JG, Chen H, Evans RM. Oxidized LDL regulates macrophage gene expression through ligand activation of PPAR $\gamma$ . *Cell*. 1998 Apr 17;93(2):229-40. doi:[10.1016/s0092-8674\(00\)81574-3](https://doi.org/10.1016/s0092-8674(00)81574-3)
8. Geeraert B, De Keyzer D, Davey PC, Cromb  F, Benhabil s N, Holvoet P. Oxidized low-density lipoprotein-induced expression of ABCA1 in blood monocytes precedes coronary atherosclerosis and is associated with plaque complexity in hypercholesterolemic pigs. *Journal of Thrombosis and Haemostasis*. 2007 Dec;5(12):2529-36. doi: [10.1111/j.1538-7836.2007.02786.x](https://doi.org/10.1111/j.1538-7836.2007.02786.x)
9. Yvan-Charvet L, Wang N, Tall AR. Role of HDL, ABCA1, and ABCG1 transporters in cholesterol efflux and immune responses. *Arteriosclerosis, thrombosis, and vascular biology*. 2010 Feb 1;30(2):139-43. doi:[10.1161/ATVBAHA.108.179283](https://doi.org/10.1161/ATVBAHA.108.179283)
10. Sankaranarayanan S, Oram JF, Asztalos BF, Vaughan AM, Lund-Katz S, Adorni MP, Phillips MC, Rothblat GH. Effects of acceptor composition and mechanism of ABCG1-mediated cellular free cholesterol efflux. *Journal of lipid research*. 2009 Feb 1;50(2):275-84. doi:[10.1194/jlr.M800362-JLR200](https://doi.org/10.1194/jlr.M800362-JLR200)
11. Gelissen IC, Harris M, Rye KA, Quinn C, Brown AJ, Kockx M, Cartland S, Packianathan M, Kritharides L, Jessup W. ABCA1 and ABCG1 synergize to mediate cholesterol export to apoA-I. *Arteriosclerosis, thrombosis, and vascular biology*. 2006 Mar 1;26(3):534-40. doi:[10.1161/01.ATV.0000200082.58536.e1](https://doi.org/10.1161/01.ATV.0000200082.58536.e1)
12. Chawla A, Boisvert WA, Lee CH, Laffitte BA, Barak Y, Joseph SB, Liao D, Nagy L, Edwards PA, Curtiss LK, Evans RM. A PPAR $\gamma$ -LXR-ABCA1 pathway in macrophages is involved in cholesterol efflux and atherogenesis. *Molecular cell*. 2001 Jan 1;7(1):161-71. doi:[10.1016/s1097-2765\(01\)00164-2](https://doi.org/10.1016/s1097-2765(01)00164-2)
13. Chawla A. Control of macrophage activation and function by PPARs. *Circulation research*. 2010 May 28;106(10):1559-69. doi:[10.1161/CIRCRESAHA.110.216523](https://doi.org/10.1161/CIRCRESAHA.110.216523)
14. Chinetti G, Lestavel S, Bocher V, Remaley AT, Neve B, Torra IP, Teissier E, Minnich A, Jaye M, Duverger N, Brewer HB. PPAR- $\alpha$  and PPAR- $\gamma$  activators induce cholesterol removal from human macrophage foam cells through stimulation of the ABCA1 pathway. *Nature medicine*. 2001 Jan;7(1):53-8. doi:[10.1038/83348](https://doi.org/10.1038/83348)
15. Bekkering S, Quintin J, Joosten LA, van der Meer JW, Netea MG, Riksen NP. Oxidized low-density lipoprotein induces long-term proinflammatory cytokine production and foam cell formation via epigenetic reprogramming of monocytes. *Arteriosclerosis, thrombosis, and vascular biology*. 2014 Aug;34(8):1731-8. doi:[10.1161/ATVBAHA.114.303887](https://doi.org/10.1161/ATVBAHA.114.303887)

16. Christ A, Günther P, Lauterbach MA, Duewell P, Biswas D, Pelka K, Scholz CJ, Oosting M, Haendler K, Baßler K, Klee K. Western diet triggers NLRP3-dependent innate immune reprogramming. *Cell*. 2018 Jan 11;172(1-2):162-75. doi:[10.1016/j.cell.2017.12.013](https://doi.org/10.1016/j.cell.2017.12.013)
17. Christ A, Bekkering S, Latz E, Riksen NP. Long-term activation of the innate immune system in atherosclerosis. In *Seminars in Immunology* 2016 Aug 1 (Vol. 28, No. 4, pp. 384-393). Academic Press. doi:[10.1016/j.smim.2016.04.004](https://doi.org/10.1016/j.smim.2016.04.004)
18. Schnack L, Sohrabi Y, Lagache SM, Kahles F, Bruemmer D, Waltenberger J, Findeisen HM. Mechanisms of trained innate immunity in oxLDL primed human coronary smooth muscle cells. *Frontiers in immunology*. 2019 Jan 23;10:13. doi:[10.3389/fimmu.2019.00013](https://doi.org/10.3389/fimmu.2019.00013)
19. Delves PJ, Roitt IM. The immune system. *New England journal of medicine*. 2000 Jul 6;343(1):37-49. doi:[10.1056/NEJM200007063430107](https://doi.org/10.1056/NEJM200007063430107)
20. Hoebe K, Janssen E, Beutler B. The interface between innate and adaptive immunity. *Nature immunology*. 2004 Oct;5(10):971-4. doi:[10.1038/ni1004-971](https://doi.org/10.1038/ni1004-971)
21. Saeed S, Quintin J, Kerstens HH, Rao NA, Aghajani-refah A, Matarese F, Cheng SC, Ratter J, Berentsen K, van der Ent MA, Sharifi N. Epigenetic programming of monocyte-to-macrophage differentiation and trained innate immunity. *science*. 2014 Sep 26;345(6204). doi:[10.1126/science.1251086](https://doi.org/10.1126/science.1251086)
22. van der Heijden CD, Noz MP, Joosten LA, Netea MG, Riksen NP, Keating ST. Epigenetics and trained immunity. *Antioxidants & redox signaling*. 2018 Oct 10;29(11):1023-40. doi:[10.1089/ars.2017.7310](https://doi.org/10.1089/ars.2017.7310)
23. Clapier CR, Cairns BR. The biology of chromatin remodeling complexes. *Annual review of biochemistry*. 2009 Jul 7;78:273-304. doi:[10.1146/annurev.biochem.77.062706.153223](https://doi.org/10.1146/annurev.biochem.77.062706.153223)
24. Kleinnijenhuis J, Quintin J, Preijers F, Joosten LA, Ifrim DC, Saeed S, Jacobs C, van Loenhout J, de Jong D, Stunnenberg HG, Xavier RJ. Bacille Calmette-Guerin induces NOD2-dependent nonspecific protection from reinfection via epigenetic reprogramming of monocytes. *Proceedings of the National Academy of Sciences*. 2012 Oct 23;109(43):17537-42. doi:[10.1073/pnas.1202870109](https://doi.org/10.1073/pnas.1202870109)
25. Kleinnijenhuis J, Quintin J, Preijers F, Benn CS, Joosten LA, Jacobs C, Van Loenhout J, Xavier RJ, Aaby P, Van Der Meer JW, Van Crevel R. Long-lasting effects of BCG vaccination on both heterologous Th1/Th17 responses and innate trained immunity. *Journal of innate immunity*. 2014;6(2):152-8. doi:[10.1159/000355628](https://doi.org/10.1159/000355628)
26. Bekkering S, van den Munckhof I, Nielen T, Lamfers E, Dinarello C, Rutten J, de Graaf J, Joosten LA, Netea MG, Gomes ME, Riksen NP. Innate immune cell activation and epigenetic remodeling in symptomatic and asymptomatic atherosclerosis in humans in vivo. *Atherosclerosis*. 2016 Nov 1;254:228-36. doi:[10.1016/j.atherosclerosis.2016.10.019](https://doi.org/10.1016/j.atherosclerosis.2016.10.019)
27. Eftimie R, Gillard JJ, Cantrell DA. Mathematical models for immunology: current state of the art and future research directions. *Bulletin of mathematical biology*. 2016 Oct;78(10):2091-134. doi:[10.1007/s11538-016-0214-9](https://doi.org/10.1007/s11538-016-0214-9)

28. Cohen A, Myerscough MR, Thompson RS. Athero-protective effects of High Density Lipoproteins (HDL): An ODE model of the early stages of atherosclerosis. *Bulletin of mathematical biology*. 2014 May 1;76(5):1117-42. doi:[10.1007/s11538-014-9948-4](https://doi.org/10.1007/s11538-014-9948-4)
29. Ougrinovskaia A, Thompson RS, Myerscough MR. An ODE model of early stages of atherosclerosis: mechanisms of the inflammatory response. *Bulletin of mathematical biology*. 2010 Aug 1;72(6):1534-61. doi:[10.1007/s11538-010-9509-4](https://doi.org/10.1007/s11538-010-9509-4)
30. Plank MJ, Wall DJ, David T. The role of endothelial calcium and nitric oxide in the localisation of atherosclerosis. *Mathematical biosciences*. 2007 May 1;207(1):26-39. doi:[10.1016/j.mbs.2006.08.017](https://doi.org/10.1016/j.mbs.2006.08.017)
31. Ibragimov AI, McNeal CJ, Ritter LR, Walton JR. A mathematical model of atherogenesis as an inflammatory response. *Mathematical Medicine and Biology*. 2005 Dec 1;22(4):305-33. doi:[10.1093/imammb/dqi011](https://doi.org/10.1093/imammb/dqi011)
32. Chalmers AD, Bursill CA, Myerscough MR. Nonlinear dynamics of early atherosclerotic plaque formation may determine the efficacy of high density lipoproteins (HDL) in plaque regression. *PloS one*. 2017 Nov 21;12(11):e0187674. doi:[10.1371/journal.pone.0187674](https://doi.org/10.1371/journal.pone.0187674)
33. Michaelis L, Menten ML. Die kinetik der invertinwirkung. *Biochem. z.* 1913 Feb;49(333-369):352.
34. Michaelis-Menten Kinetics and Briggs-Haldane Kinetics. Available from: <https://depts.washington.edu/wmatkins/kinetics/michaelis-menten.html>
35. By Thomas Shafee - Own work, CC BY 4.0, <https://commons.wikimedia.org/w/index.php?curid=38914698>
36. Falck-Hansen M, Kassiteridi C, Monaco C. Toll-like receptors in atherosclerosis. *International journal of molecular sciences*. 2013 Jul;14(7):14008-23. doi:[10.3390/ijms140714008](https://doi.org/10.3390/ijms140714008)
37. Dabagh M, Jalali P, Tarbell JM. The transport of LDL across the deformable arterial wall: the effect of endothelial cell turnover and intimal deformation under hypertension. *American Journal of Physiology-Heart and Circulatory Physiology*. 2009 Sep;297(3):H983-96. doi:[10.1152/ajpheart.00324.2009](https://doi.org/10.1152/ajpheart.00324.2009)
38. Paavola CD, Hemmerich S, Grunberger D, Polsky I, Bloom A, Freedman R, Mulkins M, Bhakta S, McCarley D, Wiesent L, Wong B. Monomeric monocyte chemoattractant protein-1 (MCP-1) binds and activates the MCP-1 receptor CCR2B. *Journal of Biological Chemistry*. 1998 Dec 11;273(50):33157-65. doi:[10.1074/jbc.273.50.33157](https://doi.org/10.1074/jbc.273.50.33157)